Oscillation of Branching Ratios Between the $D(2s)+D(1s)$ and the $D(2p)+D(1s)$ Channels in Direct Photodissociation of D_2

Jie Wang, Qingnan Meng, and Yuxiang Mo*

Department of Physics and State Key Laboratory of Low-Dimensional Quantum Physics, Tsinghua University, Beijing 100084, China

(Received 27 March 2017; revised manuscript received 24 May 2017; published 4 August 2017)

The direct photodissociation of D_2 at excitation energies above 14.76 eV occurs via two channels, $D(2s)+D(1s)$ and $D(2p)+D(1s)$. The branching ratios between the two have been measured from the dissociation threshold to 3200 cm^{-1} above it, and it is found that they show cosine oscillations as a function of the fragment wave vector magnitudes. The oscillation is due to an interference effect and can be simulated using the phase difference between the wave functions of the two channels, analogous to Young's double-slit experiment. By fitting the measured branching ratios, we have determined the depths and widths of the effective spherical potential wells related to the two channels, which are in agreement with the effective depths and widths of the *ab initio* interaction potentials. The results of this Letter illustrate the importance of the relative phase between the fragments in controlling the branching ratios of the photodissociation channels.

DOI: 10.1103/PhysRevLett.119.053002

Interference between indistinguishable pathways can lead to many interesting phenomena [1,2]. A classic example is Young's double-slit experiment with light, where the interference pattern on the viewing screen arises from the phase difference between the wave functions of the two pathways. Similar interference is also observed for matter wave, e.g., with atoms [3]. In molecular photodissociation and reaction dynamics, different channels leading to the same products may display observable quantum interference effects, such as variations of the photofragment spin-orbit state distributions with excitation photon energies, as well as reaction cross-section resonances with reactant translational collision energies [4–9]. However, interference effects arising clearly from the phase differences between the recoil fragments have rarely been observed in photodissociation, yet such effects could prove invaluable as they provide a novel insight into the quantum nature of the photodissociation process. The phase of the channel wave function plays a key role in multichannel quantum defect theory (MQDT). Jungen and his collaborators have developed and applied MQDT to the hydrogen molecule, which contributes greatly to our understanding about the Rydberg spectra, photodissociation and ionization of H_2, D_2, and HD [10–14].

The photodissociation of D_2 in the threshold region (14.76 eV) produces two channels, $D(1s)+D(2s)$ and $D(1s)+D(2p)$, which correlate mainly to the $3p\sigma B'^1\Sigma_u^+$ and $2p\sigma B^1\Sigma_u^+$ states [12–19], respectively. The wave functions of these two channels have different phase shifts relative to the free spherical waves. Extreme ultraviolet (XUV) photons can excite the ground state to the vibrational continua associated with the $3p\sigma B'^1\Sigma_u^+$ and $2p\sigma B^1\Sigma_u^+$ electronic states [15–18]. By tuning the excitation photon energies, the kinetic energies of the fragments are modified, thus resulting in a variation of the phase differences between the two channels. Oscillations of branching ratios between the two channels with excitation photon energies were predicted theoretically in 1987 [15]. In 1988, the branching ratios for H_2 were measured at seven excitation energies, using the $H(2s,2p)$ Lyman-α fluorescence method [16]. However, cosine oscillations of branching ratios have not yet been observed experimentally.

In this Letter we report an experimental determination of the fragment branching ratios between the channels $D(2p)+D(1s)$ and $D(2s)+D(1s)$ in the direct dissociation of D_2. An oscillatory dependence with excitation energies is observed, and its physics can be understood using a simple model assuming effective spherical potential wells as proxies for the *ab initio* potential energy curves (PECs).

The experimental setup consists of a tunable XUV laser pump, a UV laser probe system (364 nm), and a typical molecular beam machine equipped with a velocity map imaging component, as described elsewhere [20–22]. The tunable coherent XUV light was produced by resonance-enhanced four-wave sum mixing in a pulsed Kr jet. The branching ratio $D(2s)/[D(2s)+D(2p)]$ was determined by measuring the $D(2s,2p)$ signals as a function of the time delay between the XUV pump and the UV probe laser pulses under field-free conditions (delay-time curve). The electric field to extract the D^+ ions was applied about 200 ns after the XUV laser pulse. Because there is a large lifetime difference between the $D(2s)$ (0.14 s) and $D(2p)$ (1.6 ns) states, the branching ratio can be determined using a simulation considering this difference and the pulse time widths of the pump and probe lasers (~6 ns).

Figure 1 shows a typical example of how the delay-time curve samples the branching ratio. It is noted that predissociations also occur above the threshold, as shown by the strong peaks in Fig. 2(a) in the $D(2s,2p)$ fragment yield spectra. The measured branching ratios $D(2s)/[D(2s)+D(2p)]$, shown in Fig. 2(b), are for the

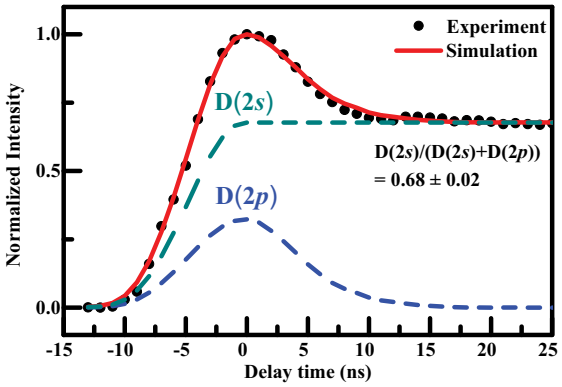

FIG. 1. Fragment $D(2s, 2p)$ intensities as a function of the time delay between the XUV pump and the UV probe laser pulses under field-free conditions. The XUV pump laser is set at 119 689.0 cm^{-1}, or 659.3 cm^{-1} above the $D(1s) + D(2s)$ dissociation threshold.

direct dissociations. Previously reported theoretical branching ratios [15] are also included in Fig. 2(b) for comparison. The theoretical calculations were carried out for the s-waves, $J' = 0$. Pure s-waves cannot be generated experimentally, because the transitions $P(1)$ ($J' = 0 \leftarrow J'' = 1$) and $R(1)$ ($J' = 2 \leftarrow J'' = 1$) are excited simultaneously and cannot be discriminated. Our experimental data that arise mainly from the $R(0)$ ($J' = 1 \leftarrow J'' = 0$) transitions correspond to the p-waves. The supersonic D_2 molecular beam consists of the rotational levels $J'' = 0$, 1, 2, and 3, with approximate population ratios of 0.53:0.30:0.13:0.03, respectively, determined chiefly by nuclear spin statistics (ortho:para = 2:1). For the first eight points shown in Fig. 2(b), the branching ratios correspond to pure $R(0)$ transitions, as transitions starting from the $J'' > 0$ rotational states were excluded. This was done from combined measurements of the delay-time curves and the velocity map images (VMIs) of the $D(2s, 2p)$ fragments under electric field and field-free conditions, respectively. The VMIs were used to determine the relative contributions of $J'' = 0$ to higher rotational states. Further details can be found in the Supplemental Material [23]. Regarding the branching ratios for the higher excitation energies in Fig. 2(b), unfortunately the resolution of the VMIs was not good enough to resolve the rotational states. In such cases, the measured branching ratios were mainly determined from $J'' = 0$ and 1, whose energy difference is 60 cm^{-1}. The branching ratio is mainly determined from the kinetic energies of the fragments [15]. For fragments with kinetic energies 283 cm^{-1} above the threshold [the ninth point in Fig. 2(b)], $J'' = 1$ has only a small effect on the branching ratios. For instance, for the eighth point with a kinetic energy of 223 cm^{-1}, the effect of $J'' > 0$ states on the branching ratio is only +0.04 (see [23]). It is therefore assumed, in the following discussion, that our measured branching ratios are those of the $R(0)$ transitions.

Figure 3 shows the branching ratios as a function of the wave vector magnitude k of the fragments in the

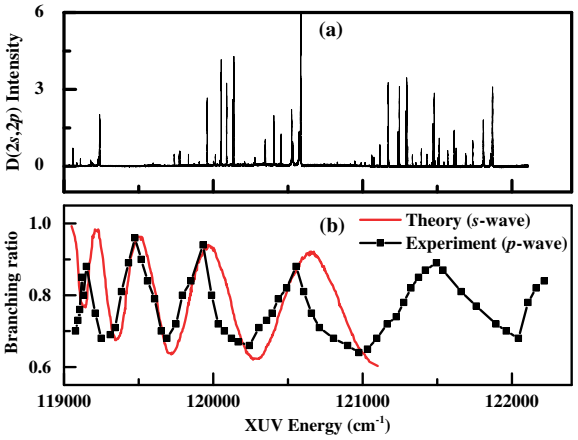

FIG. 2. (a) The $D(2s, 2p)$ fragment yield spectrum from the photodissociation of D_2. (b) The branching ratios $D(2s)/[D(2s) + D(2p)]$ from the direct dissociations of D_2. The photon energies for the measured branching ratios are set at the flat region of the fragment yield spectrum. The experimental results are for the $R(0)$ transitions (p-wave), and the theoretical results are for the $P(1)$ transitions (s-wave) [15]. The threshold for the production of $D(1s) + D(2s)$ is 119 029.7 cm^{-1} [19].

center-of-mass coordinate. $k = \sqrt{2\mu E_t}/\hbar$, where E_t is the translational energy of the fragments in the center-of-mass coordinate, μ is the reduced mass of D_2, and $\hbar$ is the reduced Planck constant. Figures 3(a) and 3(b) display the experimental branching ratios and the theoretical results of the s-wave [15], respectively. It is seen that the branching ratios as a function of the wave vector magnitudes are similar to a cosine function.

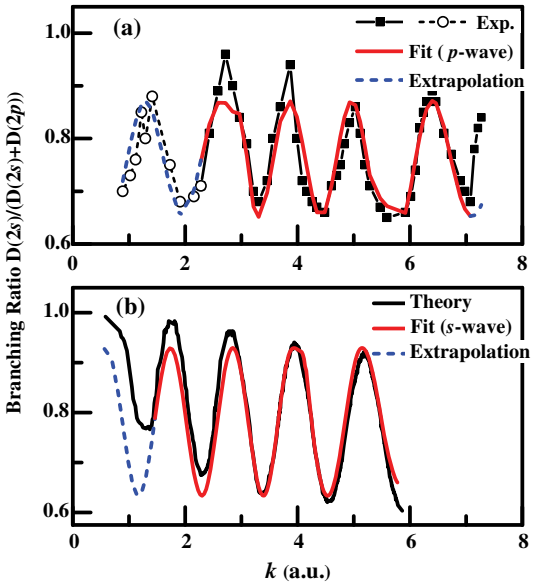

FIG. 3. (a) Experimental and (b) theoretical $D(2s)/[D(2s) + D(2p)]$ branching ratios [15]. The corresponding fits to determine the widths and depths of the effective spherical potential wells are also shown. Near the threshold region the oscillations are out of phase between the theory (s-wave) and experiment (p-wave).

TABLE I. Widths $\tilde{a}$ and depths $\tilde{U}$ of the effective spherical potential wells corresponding to the potential energy curves of the $2p\sigma B^1\Sigma_u^+$ and $3p\sigma B'^1\Sigma_u^+$ states. The parameters $\tilde{r}_A$ and $\tilde{r}_B$ describe the cosine oscillation of the $D(2s)/[(D(2s)+D(2p)]$ branching ratios in the direct photodissociation of D_2.

	$\tilde{a}$ $(2p\sigma)$ (atomic units)	$-\tilde{U}$ $(2p\sigma)$ $(10^3$ cm$^{-1})$	$\tilde{a}$ $(3p\sigma)$ (atomic units)	$-\tilde{U}$ $(3p\sigma)$ $(10^3$ cm$^{-1})$	$\tilde{r}_A$[a]	$\tilde{r}_B$[a]
Theory[b]	6.46	30.6	1.81	12.0		
Theory[c]	6.4 ± 0.4	33 ± 2	1.7 ± 0.4	11 ± 3	0.79 ± 0.01	0.13 ± 0.01
Experiment[d]	6.4 ± 0.4	33 ± 5	1.6 ± 0.4	12 ± 4	0.76 ± 0.01	0.11 ± 0.01

[a]See Eq. (6).
[b]Calculated from the *ab initio* PECs [24] using Eqs. (10a) and (10b).
[c]From a fit of the theoretical results using the *s*-wave wave function [15].
[d]From a fit of the measured branching ratios using the *p*-wave wave function.

Direct photodissociation of D_2 involves excitation from the ground state to the vibrational continua of the $3p\sigma B'^1\Sigma_u^+$ and $2p\sigma B^1\Sigma_u^+$ electronic states. We use the partial wave method to describe the vibrational continuum [2]. In our discussion, we assume that the coupling between the electronic angular momentum and the nuclear rotational angular momentum is weak; therefore, only a *p*-wave ($l = 1$) is possible for a photodissociation starting from $J'' = 0$, whereby the continuum wave function is

$$\Psi_l = (2l+1)P_l(\cos\theta)R_l(r)i^l \exp(i\delta_l), \tag{1}$$

where δ_l is the phase shift of the lth wave relative to the free spherical wave, $P_l(\cos\theta)$ is the Legendre polynomial describing the angular properties of the wave function, and $R_l(r)$ is the radial wave function [2]. As we mentioned earlier, two potential energy curves of the $3p\sigma B'^1\Sigma_u^+$ and $2p\sigma B^1\Sigma_u^+$ states correlate to the $D(2s)+D(1s)$ and $D(2p)+D(1s)$ channels, respectively. The total wave functions should then be a combination of the two nuclear vibrational continua associated with these electronic states. The two resulting mixed wave functions are orthogonal [9]; one of them has a larger mixing coefficient for $3p\sigma B'^1\Sigma_u^+$, denoted as $\tilde{\Psi}_{2s}$, and the other has a larger mixing coefficient for $2p\sigma B^1\Sigma_u^+$, denoted as $\tilde{\Psi}_{2p}$, expressible as

$$\tilde{\Psi}_{2s} = c_{2s}\exp(i\delta_1(2s))[P_1(\cos\theta)R_{1(2s)}(r)]|3p\sigma\rangle + c_{2p}\exp(i\delta_1(2p))[P_1(\cos\theta)R_{1(2p)}(r)]|2p\sigma\rangle \tag{2a}$$

$$\tilde{\Psi}_{2p} = -c_{2p}\exp(i\delta_1(2s))[P_1(\cos\theta)R_{1(2s)}(r)]|3p\sigma\rangle + c_{2s}\exp(i\delta_1(2p))[P_1(\cos\theta)R_{1(2p)}(r)]|2p\sigma\rangle \tag{2b}$$

c_{2p} and c_{2s} are the mixing coefficients that can be determined by solving the close-coupled Schrödinger equation [15] or, alternatively, using MQDT [10–14]. The excitation cross section from the ground state of D_2 ($|g\rangle$) to $\tilde{\Psi}_{2s}$ is proportional to

$$\begin{aligned}|\langle g|d|\tilde{\Psi}_{2s}\rangle|^2 &= |c_{2p}|^2\langle g|d_{2p}|P_1(\cos\theta)R_{1(2p)}(r)\rangle^2 + |c_{2s}|^2\langle g|d_{2s}|P_1(\cos\theta)R_{1(2s)}(r)\rangle^2 \\ &\quad + 2\cos(\delta_{1(2s)}-\delta_{1(2p)})c_{2p}c_{2s}\langle g|d_{2p}|P_1(\cos\theta)R_{1(2p)}(r)\rangle\langle g|d_{2s}|P_1(\cos\theta)R_{1(2s)}(r)\rangle \\ &= |c_{2p}|^2\tilde{d}_{2p}^2 + |c_{2s}|^2\tilde{d}_{2s}^2 + 2\cos(\delta_{1(2s)}-\delta_{1(2p)})c_{2p}c_{2s}\tilde{d}_{2p}\tilde{d}_{2s},\end{aligned} \tag{3a}$$

where d_{2s} and d_{2p} are the electronic transition dipole moments, and $\tilde{d}_{2s}^2$ and $\tilde{d}_{2p}^2$ are the transition intensities from the ground electronic state to the $3p\sigma B'^1\Sigma_u^+$ and $2p\sigma B^1\Sigma_u^+$ states, respectively. The excitation to $\tilde{\Psi}_{2p}$ state is

$$\begin{aligned}|\langle g|d|\tilde{\Psi}_{2p}\rangle|^2 &= |c_{2s}|^2\tilde{d}_{2p}^2 + |c_{2p}|^2\tilde{d}_{2s}^2 \\ &\quad - 2\cos(\delta_{1(2s)}-\delta_{1(2p)})c_{2p}c_{2s}\tilde{d}_{2p}\tilde{d}_{2s}.\end{aligned} \tag{3b}$$

Both $\tilde{\Psi}_{2p}$ and $\tilde{\Psi}_{2s}$ contain the probabilities for the production of the $D(2s)+D(1s)$ channel, so the total cross section to observe this channel is proportional to

$$\begin{aligned}\tilde{\sigma}_{2s} &= c_{2s}^2|\langle g|d_{2s}|\tilde{\Psi}_{2s}\rangle|^2 + c_{2p}^2|\langle g|d_{2p}|\tilde{\Psi}_{2p}\rangle|^2 \\ &= \tilde{A} + \tilde{B}\cos(\delta_{1(2s)}-\delta_{1(2p)}),\end{aligned} \tag{4a}$$

$$\tilde{A} = c_{2s}^2[c_{2s}^2\tilde{d}_{2s}^2 + c_{2p}^2\tilde{d}_{2p}^2] + c_{2p}^2[c_{2s}^2\tilde{d}_{2p}^2 + c_{2p}^2\tilde{d}_{2s}^2], \tag{4b}$$

$$\tilde{B} = 2c_{2p}c_{2s}\tilde{d}_{2p}\tilde{d}_{2s}[c_{2s}^2 - c_{2p}^2]. \tag{4c}$$

As can be seen in Eqs. (4b) and (4c), $\tilde{A}$ and $\tilde{B}$ are related to the mixing coefficients and transition intensities. Similarly,

$$\tilde{\sigma}_{2p} = \tilde{A}' - \tilde{B}\cos(\delta_{1(2s)} - \delta_{1(2p)}), \tag{5a}$$

$$\tilde{A}' = c_{2p}^2[c_{2s}^2\tilde{d}_{2s}^2 + c_{2p}^2\tilde{d}_{2p}^2] + c_{2s}^2[c_{2s}^2\tilde{d}_{2p}^2 + c_{2p}^2\tilde{d}_{2s}^2]. \tag{5b}$$

The total cross section for the two channels is proportional to $\tilde{d}_{2p}^2 + \tilde{d}_{2s}^2$, as derived from Eqs. (4b) and (5b), which we assume to be a constant [15]. The branching ratio, $D(2s)/[D(2s) + D(2p)]$, is represented by

$$\begin{aligned}\frac{\tilde{\sigma}_{2s}}{\tilde{\sigma}_{2s} + \tilde{\sigma}_{2B}} &= \frac{\tilde{A}}{\tilde{A} + \tilde{A}'} + \frac{\tilde{B}}{\tilde{A} + \tilde{A}'}\cos(\delta_{1(2s)} - \delta_{1(2p)}) \\ &= \tilde{r}_A + \tilde{r}_B\cos(\delta_{1(2s)} - \delta_{1(2p)}),\end{aligned} \tag{6}$$

where $\tilde{r}_A$ is the branching ratio when the two scattering functions are out of phase ($\pi/2$), and $\tilde{r}_B$ may be regarded as the modulation depth of the branching ratio as a function of the phase.

Although the phase difference in Eq. (6) can be calculated exactly [10–15], we emphasize the main physics here with an effective potential model that may be regarded in essence an application of MQDT [10,11]. In this model, the diatomic interaction potentials are assumed to be spherical potential wells, characterized by depth $-\tilde{U}$ and width $\tilde{a}$. For the p-wave, the phase shift relative to a free spherical wave can be derived using standard quantum mechanical formalism [2],

$$\delta_1 = -k\tilde{a} + \cot^{-1}\left(\frac{1}{\tilde{a}k} - \frac{k}{\tilde{a}\tau^2} + \frac{k\cot\tau\tilde{a}}{\tau}\right), \tag{7a}$$

where $\tau = \sqrt{2u(E_t + \tilde{U}_0)}/\hbar$. In our case, $\tau \gg k$. If $\tilde{a}k \gg 1$, we have

$$\delta_1 \approx -k\tilde{a} + \cot^{-1}\left(\frac{k\cot\tau\tilde{a}}{\tau}\right). \tag{7b}$$

For the case we study, the wave vectors of the two channels are nearly equal, so the phase difference between them becomes

$$\begin{aligned}\delta_{1(2p)} - \delta_{1(2s)} \approx -k(\tilde{a}_{2p} - \tilde{a}_{2s}) &+ \cot^{-1}\left(\frac{k\cot\tau_{2p}\tilde{a}_{2p}}{\tau_{2p}}\right) \\ &- \cot^{-1}\left(\frac{k\cot\tau_{2s}\tilde{a}_{2s}}{\tau_{2s}}\right).\end{aligned} \tag{8}$$

The calculations show in the above equation that the first term is dominant [23]. Therefore, the phase difference is determined mainly by the wave vector k, which provides a theoretical explanation for the experimental result, namely, that the branching ratio is a cosine function of the wave vector [15].

Using Eqs. (6) and (7b), we fitted the measured branching ratios employing the nonlinear least-squares method. The result is shown in Fig. 3(a). It is seen that the fit reproduces quite well the experimental results. The branching ratios in the lower and higher values of the wave vectors were not included in the fit, but the extension of the curves to the low-k values describes the trend of the experimental results very well. From the fit, the $\tilde{U}$ and $\tilde{a}$ values of the two spherical potential wells are obtained, and are listed in Table I, along with the parameters $\tilde{r}_A$ and $\tilde{r}_B$ in Eq. (6).

In addition to the fit of the experimental branching ratios for the $R(0)$ transitions, we also fitted the theoretical branching ratios of the $P(1)$ transitions (s-wave). The expression for the phase shift of an s-wave is [2]

$$\delta_0 = -k\tilde{a} + \arctan\left(\frac{k\tan\tau\tilde{a}}{\tau}\right) \tag{9}$$

The fitted curve is shown in Fig. 3(b). For $k > 2.0$, the fitted curve agrees well with the theoretical calculations. The determined $\tilde{a}$ and $\tilde{U}$ values are nearly the same as those resulting from the measured branching ratios. Notice that the branching ratio oscillations of the s- and p-waves are out of phase in the threshold region.

For a comparison of the effective spherical potential wells extracted from the experimental data, with those of the *ab initio* PECs, we assume that the effective width $\tilde{a}$ and depth $\tilde{U}$ for a theoretical PEC $[U(r)]$ can be approximated by

$$\tilde{a} = \frac{\int_0^\infty rU(r)r^2dr}{\int_0^\infty U(r)r^2dr}, \tag{10a}$$

$$-\tilde{U} = \frac{\int_0^\infty 4\pi U(r)r^2dr}{(4/3)\pi\tilde{a}^3}. \tag{10b}$$

The starting point of the effective potential $r = 0$ in the above corresponds to an internuclear distance of $R = 1.0$ a.u., where the potential is very large. The results are listed in Table I. It is seen that the parameters of the effective potential wells extracted from the fit of the experimental data are in good agreement with those resulting from the *ab initio* PECs [24]. For example, the widths $\tilde{a}$ of the $2p\sigma B^1\Sigma_u^+$ and $3p\sigma B'^1\Sigma_u^+$ states, resulting from the fits, are 6.4 ± 0.4 and 1.6 ± 0.4 a.u., vs. the values of 6.46 and 1.81 a.u. derived from the *ab initio* PECs. The large width of the $2p\sigma B^1\Sigma_u^+$ state relative to that of the $3p\sigma B'^1\Sigma_u^+$ state is because the former includes some ion-pair state character and, hence, has a much longer equilibrium bond length than typical covalent bonds [25,26].

Figure 4 shows the PECs of the $2p\sigma B^1\Sigma_u^+$ and $3p\sigma B'^1\Sigma_u^+$ states, the corresponding effective spherical potential wells, and the scattering wave functions calculated using the effective spherical potential wells. It is clearly seen that the effective potentials can satisfactorily describe the main properties of the PECs. For kinetic energies (wave vectors) of $E_t = 902$ cm^{-1} ($k = 3.87$ a.u.) and $E_t = 656$ cm^{-1} ($k = 3.30$ a.u.), the wave functions for the $2p\sigma B^1\Sigma_u^+$

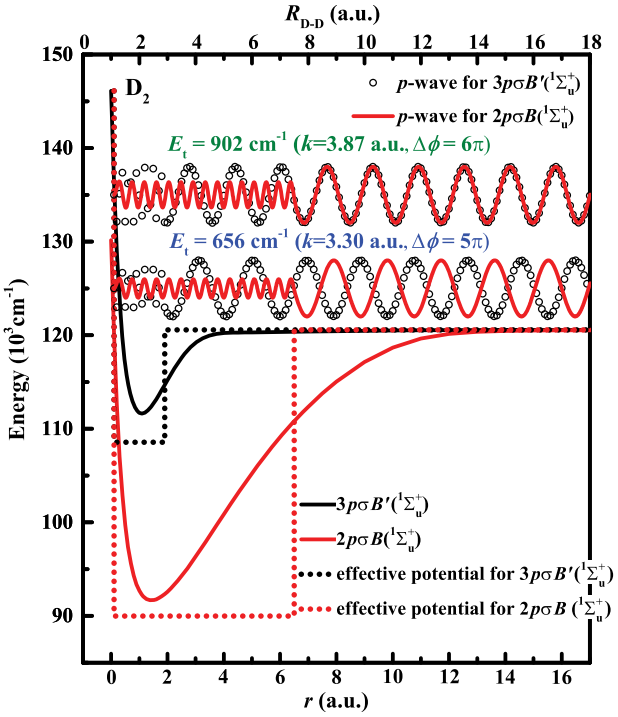

FIG. 4. PECs of the $3p\sigma B'^1\Sigma_u^+$ and $2p\sigma B^1\Sigma_u^+$ states of D_2 [24], and the corresponding effective spherical potential wells determined from the fit of the measured branching ratios. Two scattering p-wave functions for the effective spherical potential wells are also shown. The wave functions are calculated by $r[\sin(\tau r)/(\tau r)^2 - \cos(\tau r)/\tau r]$ and $r[\sin(kr+\delta_1)/(kr)^2 - \cos(kr+\delta_1)/kr]$ inside and outside of the wells, respectively. δ_1 is the phase shift.

and $3p\sigma B'^1\Sigma_u^+$ states are in phase and out of phase, respectively, which results in observed maximum (0.94 ± 0.02) and minimum (0.68 ± 0.02) values for the $D(2s)/[D(2s) + D(2p)]$ branching ratios.

In summary, the branching ratios between the channels $D(2s) + D(1s)$ and $D(2p) + D(1s)$ in the direct photodissociation of D_2 have been measured and are found to be described by a cosine function of the fragment wave vectors. The oscillation is understood to arise from the phase differences between the wave functions of the two dissociation channels, which confirms a previous theoretical prediction [15]. The parameters of the effective spherical potentials were determined by fitting the measured branching ratios. The results obtained in this Letter demonstrate clearly that the relative phase between the fragments of the two photodissociation channels significantly modulates the corresponding branching ratio. The presently introduced delay-time-curve technique to measure the branching ratio $D(2s)/[D(2s) + D(2p)]$ can be applied to study the photodissociation dynamics of other molecules.

We are grateful to Dr. Gabriel J. Vázquez of the Universidad Nacional Autonóma de México for carefully reading the manuscript and making valuable suggestions. This work is funded by Projects No. 11274196 and No. 21327902 supported by the National Science Foundation of China, and Project No. 2013CB834604 supported by the Ministry of Science and Technology of China.

*ymo@mail.tsinghua.edu.cn

[1] C. Cohen-Tannoudji and D. Guéry-Odelin, *Advances in Atomic Physics: An Overview* (World Scientific, New Jersey, 2011).
[2] B. H. Bransden and C. J. Joachain, *Physics of Atoms and Molecules* (Pearson Education Limited, London, 2003).
[3] O. Carnal and J. Mlynek, Phys. Rev. Lett. **66**, 2689 (1991).
[4] P. Brumer and M. Shapiro, Acc. Chem. Res. **22**, 407 (1989).
[5] L. Zhu, V. Kleiman, X. Li, S. Lu, and R. J. Gordon, Science **270**, 77 (1995).
[6] P. M. Regan, S. R. Langford, A. J. Orr-Ewing, and M. N. R. Ashfold, J. Chem. Phys. **110**, 281 (1999).
[7] D. Dai, C. C. Wang, S. A. Harich, X. Wang, X. Yang, S. D. Chao, and R. T. Skodje, Science **300**, 1730 (2003).
[8] P. G. Jambrina, D. Herráez-Aguilar, F. J. Aoiz, M. Sneha, J. Jankunas, and R. N. Zare, Nat. Chem. **7**, 661 (2015).
[9] H. Lefebvre-Brion and R. W. Field, *The Spectra and Dynamics of Diatomic Molecules* (Elsevier Academy Press, Amsterdam, 2004).
[10] Ch. Jungen, in *Handbook of High-Resolution Spectroscopy*, edited by M. Quack and F. Merkt (John Wiley & Sons, Hoboken, 2011).
[11] Ch. Jungen and S. C. Ross, Phys. Rev. A **55**, R2503 (1997).
[12] H. Gao, Ch. Jungen, and C. H. Greene, Phys. Rev. A **47**, 4877 (1993).
[13] J. Zs. Mezei, I. F. Schneider, M. Glass-Maujean, and Ch. Jungen, J. Chem. Phys. **141**, 064305 (2014).
[14] M. Sommavilla, F. Merkt, J. Zs. Mezei, and Ch. Jungen, J. Chem. Phys. **144**, 084303 (2016).
[15] J. A. Beswick and M. Glass-Maujean, Phys. Rev. A **35**, 3339 (1987).
[16] M. Glass-Maujean, H. Frohlich, and J. A. Beswick, Phys. Rev. Lett. **61**, 157 (1988).
[17] M. Glass-Maujean and J. A. Beswick, Phys. Rev. A **38**, 5660 (1988).
[18] E. Flemming, O. Wihelmi, H. Schmoranzer, and M. Glass-Maujean, J. Chem. Phys. **103**, 4090 (1995).
[19] E. E. Eyler and N. Melikechi, Phys. Rev. A **48**, R18 (1993).
[20] Y. Zhou, Q. Meng, and Y. Mo, J. Chem. Phys. **141**, 014301 (2014).
[21] Q. Meng and Y. Mo, J. Chem. Phys. **144**, 154305 (2016).
[22] Q. Meng, J. Wang, and Y. Mo, Phys. Rev. A **93**, 050501 (2016).
[23] See Supplemental Material at http://link.aps.org/supplemental/10.1103/PhysRevLett.119.053002 for the experimental branching ratios and the discussion on Eq. (8).
[24] L. Wolniewicz and K. Dressler, J. Chem. Phys. **88**, 3861 (1988).
[25] C. Zhou, Y. Hao, and Y. Mo, J. Phys. Chem. A **112**, 8263 (2008).
[26] C. Zhou and Y. Mo, J. Chem. Phys. **139**, 084314 (2013).